α-cluster structure in even-even nuclei around ^{94}Mo

M. A. Souza[1,2,*] and H. Miyake[1,†]

[1]*Instituto de Física, Universidade de São Paulo, Rua do Matão, Travessa R, 187, CEP 05508-090,*
Cidade Universitária, São Paulo - SP, Brazil

[2]*Instituto Federal de Educação, Ciência e Tecnologia de São Paulo - Campus São Paulo, Rua Pedro Vicente, 625,*
CEP 01109-010, Canindé, São Paulo - SP, Brazil

[Background] The α-cluster model was successful for describing spectroscopic properties of light nuclei near the shell closures. Evidences of the α-cluster structure in ^{94}Mo were shown, motivating the search for the same structure in other intermediate mass nuclei. [Purpose] The systematic analysis of the α-cluster structure in ^{94}Mo and four even-even neighboring nuclei. [Method] The α-cluster model with the local potential approach. [Results] A good general description of the experimental ground state bands is obtained with only one variable parameter. It is shown that the employed α + core potential is weakly dependent on the angular momentum L and such dependence may be described satisfactorily by a simple L-dependent factor for the five nuclei. The radial parameter of the α + core potential reveals a linear trend in relation to the total nuclear radius and the sum of the α-cluster and core radii. The calculated $B(E2)$ transition rates reproduce correctly the order of magnitude of almost all experimental data without the use of effective charges. The rms intercluster separations and reduced α widths obtained for the ground state bands point to a reduction of the α-cluster intensity with the increasing spin. Negative parity bands are calculated and compared to available experimental levels. The volume integral per nucleon pair and rms radii were calculated for the studied α + core potentials, revealing a similarity with the real parts of the optical potentials used to describe the $\alpha + {}^{90}$Zr and $\alpha + {}^{92}$Mo elastic scattering at several energies. [Conclusions] This work strongly indicates the presence of similar α + core structures for the $N = 52$ even-even nuclei of the Mo region.

I. INTRODUCTION

The α-cluster structure is an important aspect in the analysis of nuclear spectral data. The cluster interpretation represents a suitable way to describe nuclear states which could be investigated by more complex microscopic treatments. The α-cluster model has been successful in reproducing several levels of the energy spectra, electromagnetic properties, α-emission widths, and α-particle elastic scattering data in nuclei near the double shell closures. The α-cluster interpretation has often been used in studies on different mass regions. In heavy and superheavy mass regions, recent studies use this concept for analysis of the α-decay phenomenon [1–4]. In the light mass region, the α-cluster interpretation is combined with various approaches for describing properties of $n\alpha$ or $n\alpha + \{$other particles$\}$ nuclei; recent examples are the concept of nonlocalized clustering [5], the Hartree-Fock-Bogoliubov approach [6], and the quantum molecular dynamics (or its antisymmetrized version) [7,8].

The earlier works of Buck, Dover, and Vary [9] on ^{16}O and ^{20}Ne, and Michel, Reidemeister, and Ohkubo [10] on ^{44}Ti, demonstrated the success of the α-cluster interpretation with the local potential model (LPM) to describe the first experimental energy bands of the three nuclei. The model was also used to determine the $B(E2)$ transition rates between the members of the calculated bands, obtaining good agreement

with the experimental data without the use of effective charges. The calculated α-decay widths for ^{16}O and ^{20}Ne [9] provide a good reproduction of the orders of magnitude of the respective experimental widths. The subsequent work of Buck, Merchant, and Perez [11], which takes a modified Woods-Saxon potential (W.S.+W.S.^{3}) for the α + core interaction, confirmed the favorable results for the nuclei ^{20}Ne and ^{44}Ti.

The study of the α-cluster structure above double shell closures continued in the heavier nuclei ^{94}Mo and ^{212}Po. Concerning ^{94}Mo, Ref. [11] describes the $\alpha + {}^{90}$Zr system through the nuclear W.S. + W.S.^{3} potential, where a set of fixed parameters is employed for nuclei of different mass regions. The results yield a good description of the ground state band of ^{94}Mo and the correct order of magnitude of the experimental $B(E2)$ rates without the use of effective charges [11]. The work of Ohkubo [12] analyzes the same structure in ^{94}Mo through a double folding potential; in this case, a good description of the $\alpha + {}^{90}$Zr elastic scattering data is obtained, the ^{94}Mo ground state band is reproduced with a weak dependence on the quantum number L, and the absolute values of the $B(E2)$ transition rates are well described with a small effective charge ($\delta e = 0.2e$). Following works of Michel *et al.* [13] and Souza and Miyake [14] reinforce the indications on the α-cluster structure in the ^{94}Mo states. Concerning ^{212}Po, the results obtained in Refs. [11,12,15,16] for the ground state band and the $\alpha + {}^{208}$Pb elastic scattering cross sections show a similar level of agreement with the respective experimental data. Additionally, the model provides a satisfactory description of the orders of magnitude of the experimental half-lives $T_{1/2}$ for ^{212}Po.

*marsouza@if.usp.br

†miyake@if.usp.br

The work of Mohr [17] shows a study of the $\alpha +$ core structure in intermediate mass nuclei by means of a double folding nuclear potential. Using the LPM, the calculations give favorable results for the $B(E2)$ rates of the ground state bands. However, an analysis of the intensity parameter λ of the nuclear potential shows a weak L dependence and a significant dependence on the proton number of the nucleus, mainly around the $Z = 40$ subshell closure and the $Z = 50$ shell closure.

In this context, the purpose of the present work is a detailed analysis of the α-cluster structure in ^{94}Mo and the even-even neighboring nuclei ^{90}Sr, ^{92}Zr, ^{96}Ru, and ^{98}Pd. The $\alpha +$ core systems are calculated from the viewpoint of the LPM. Several properties of the ground state bands are discussed and indications of $\alpha +$ core negative parity bands are sought. Possible structure patterns in these nuclei are investigated.

II. SELECTION OF PREFERENTIAL NUCLEI FOR α CLUSTERING

A preliminary question is the choice of a criterion to determine the most favorable nuclei for α-clustering in a specified mass region. An usual procedure is the selection of nuclei with the configuration of α-cluster plus doubly (or even singly) closed shell core. However, such procedure does not allow for a systematic analysis of any set of nuclei. In this work, we use a criterion based only on experimental data of binding energy [18]. An appropriate quantity for comparing different nuclei of a set is the variation of average binding energy per nucleon of the system due to the $\alpha +$ core decomposition. This value is given by

$$\frac{Q_\alpha}{A_T} = \frac{B_\alpha + B_{\text{core}} - B_T}{A_T}, \qquad (1)$$

where Q_α is the Q value for α separation, A_T is the mass number of the total nucleus, and B_α, B_{core}, and B_T are the experimental binding energies of the α cluster, the core, and the total nucleus, respectively. Thus, an absolute (or local) maximum of Q_α/A_T indicates the preferred nucleus for α-clustering in comparison with the rest of (or neighboring) nuclei in the set.

Restricted atomic number and mass number regions are defined around ^{94}Mo for the α-cluster analysis. The Q_α/A_T value is used for comparison of even-even isotopes between $Z = 38$ and $Z = 46$, and even-even isobars between $A = 90$ and $A = 98$. Figure 1 shows graphically the Q_α/A_T values for different sets of nuclei. Observing the sets of even-even isotopes, a local Q_α/A_T peak is seen for ^{90}Sr and absolute Q_α/A_T peaks are seen for ^{92}Zr, ^{94}Mo, ^{96}Ru, and ^{98}Pd. Observing the sets of even-even isobars, local Q_α/A_T peaks are seen for ^{90}Sr and ^{92}Zr, and absolute Q_α/A_T peaks are seen for ^{94}Mo, ^{96}Ru, and ^{98}Pd. Such results imply that ^{90}Sr, ^{92}Zr, ^{94}Mo, ^{96}Ru, and ^{98}Pd are preferential nuclei for α clustering if they are compared with the respective even-even isotopes and isobars simultaneously.

It is important to note that the five mentioned nuclei have the same number of neutrons ($N = 52$), that is, their cores have the same magic number $N = 50$. Therefore, the Q_α/A_T analysis provides a strong indication that the number
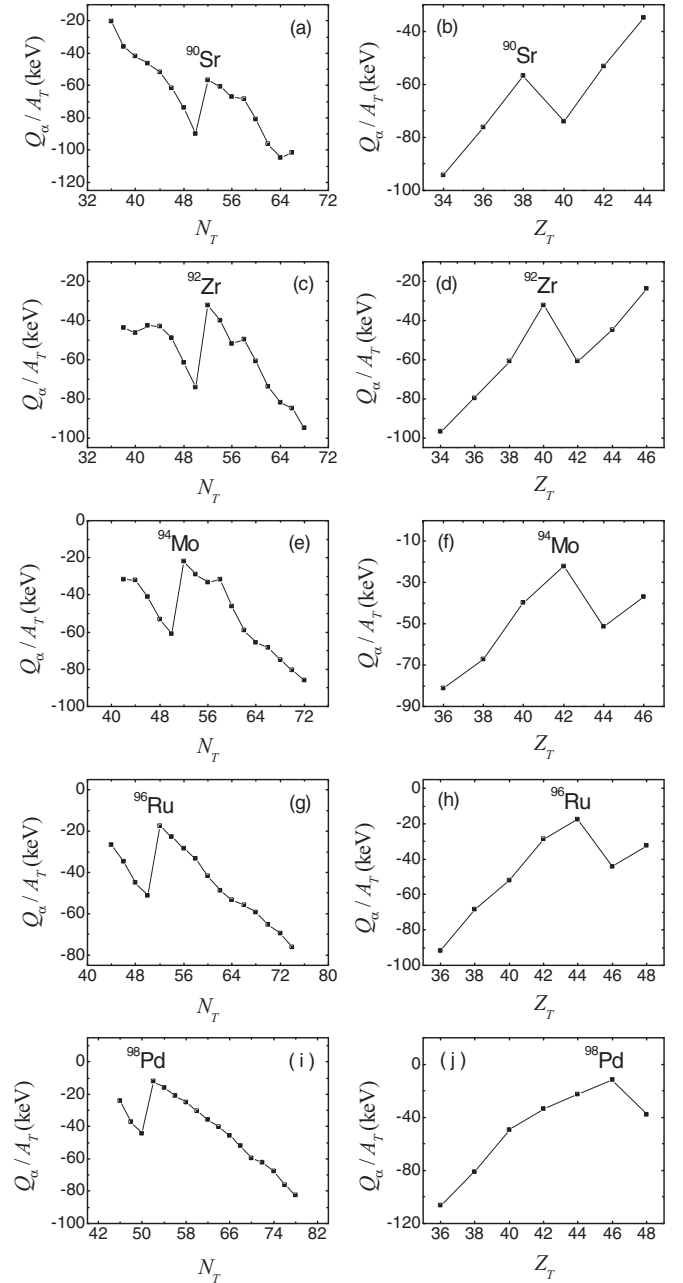

FIG. 1. Q_α/A_T values obtained for the $\alpha +$ core decomposition of even-even Sr (a), Zr (c), Mo (e), Ru (g), and Pd (i) isotopes as a function of the total neutron number N_T, and even-even $A = 90$ (b), $A = 92$ (d), $A = 94$ (f), $A = 96$ (h), and $A = 98$ (j) isobars as a function of the total charge number Z_T. The Q_α/A_T peaks corresponding to ^{90}Sr, ^{92}Zr, ^{94}Mo, ^{96}Ru, and ^{98}Pd are indicated.

$N_{\text{core}} = 50$ characterizes the most favorable nuclei for α clustering in the Mo mass region.

A comparison of the Q_α/A_T values for the set of even-even $N = 52$ isotones is presented in Fig. 2. It is noted that the Q_α/A_T variation rate increases moderately between $Z_T = 38$ and $Z_T = 40$ in comparison with other neighboring nuclei. Therefore, the effect of the subshell closure at $Z_{\text{core}} = 38$ is more pronounced than at $Z_{\text{core}} = 40$ for the increase of
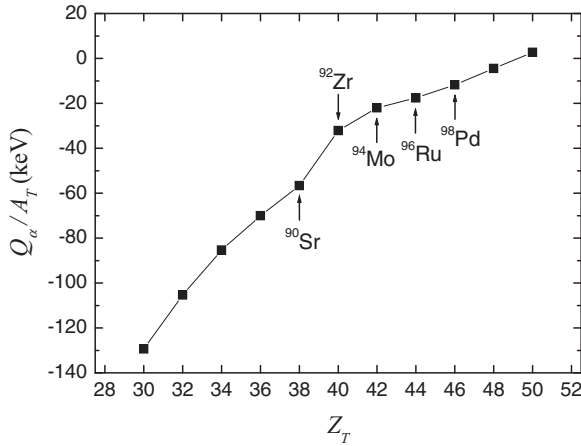
FIG. 2. Q_α/A_T values obtained for the α + core decomposition of even-even $N = 52$ isotones as a function of the total charge number Z_T. The dots corresponding to ^{90}Sr, ^{92}Zr, ^{94}Mo, ^{96}Ru, and ^{98}Pd are indicated.

Q_α/A_T. The fact that there are no abrupt Q_α/A_T variations around ^{94}Mo suggests that this nucleus and its neighboring isotones should present similar α + core structures. Indeed, this indication is verified by different properties discussed in Sec. IV.

III. α-CLUSTER MODEL

The properties of the nucleus are viewed in terms of a preformed α-particle orbiting an inert core. Internal excitations of the α cluster and the core are not considered in the calculations. The α + core interaction is described through a local phenomenological potential $V(r) = V_C(r) + V_N(r)$ containing the Coulomb and nuclear terms. For the nuclear potential, we adopt the form

$$V_N(r) = -V_0 \left\{ \frac{b}{1 + \exp[(r - R)/a]} + \frac{1 - b}{\{1 + \exp[(r - R)/3a]\}^3} \right\} \quad (2)$$

proposed by Buck, Merchant, and Perez [11]. The Coulomb potential $V_C(r)$ is taken to be that of a uniform spherical charge distribution of radius $R_C = R$. The inclusion of the centrifugal term results in the effective potential

$$V_{\text{eff}}(r) = V(r) + \frac{L(L + 1)\hbar^2}{2\mu r^2}, \quad (3)$$

where μ is the reduced mass of the α + core system.

The general description of the ground state bands is made with the fixed parameters $V_0 = 220$ MeV, $a = 0.65$ fm, and $b = 0.3$, while R is fitted separately for each nucleus. The values of V_0, a, and b, which are obtained from Ref. [11], have been fitted to reproduce satisfactorily the experimental excitation energies of the ground state bands of ^{20}Ne, ^{44}Ti, ^{94}Mo, and ^{212}Po, as well as the experimental α-decay half-lives for several even-even heavy nuclei. Using a procedure similar to that employed in Ref. [11], the radial parameter R is fitted in the present work to reproduce the experimental 4^+ member

TABLE I. Values of the radial parameter R for the intermediate mass nuclei analysed in this work.

Nucleus	System	R (fm)
^{90}Sr	$\alpha + {}^{86}$Kr	5.321
^{92}Zr	$\alpha + {}^{88}$Sr	5.295
^{94}Mo	$\alpha + {}^{90}$Zr	5.784
^{96}Ru	$\alpha + {}^{92}$Mo	5.808
^{98}Pd	$\alpha + {}^{94}$Ru	5.825

of the ground state band of each nucleus. The obtained values for R are shown in Table I.

The Pauli principle requirements for the α valence nucleons are introduced through the quantum number

$$G = 2N + L, \quad (4)$$

where N is the number of internal nodes in the radial wave function and L is the orbital angular momentum. The global quantum number G identifies the bands of states. In this way, the restriction $G \geqslant G_{\text{g.s.}}$ is applied, where $G_{\text{g.s.}}$ corresponds to the ground state band. The value $G_{\text{g.s.}} = 14$ is employed for ^{90}Sr and ^{92}Zr, and $G_{\text{g.s.}} = 16$ for ^{94}Mo, ^{96}Ru, and ^{98}Pd. These two values are obtained from the Wildermuth condition [19] considering the $(pf)^2(sdg)^2$ and $(sdg)^4$ configurations, respectively.

The energy levels and associated radial wave functions are calculated by solving the Schrödinger radial equation for the reduced mass of the α + core system.

IV. RESULTS

A. Parameter R

Table I presents an increase of the parameter R with the nuclear mass number, except to a decrease from ^{90}Sr to ^{92}Zr. Such a feature motivates the search for a relation of R to the nuclear radius. Figure 3(a) shows R as a function of $A_T^{1/3}$ and Fig. 3(b) as a function of $A_\alpha^{1/3} + A_{\text{core}}^{1/3}$, where A_T, A_α, and A_{core} are the mass numbers of the total nucleus, the α particle, and the core, respectively. Figure 3(a) confirms the increasing trend of R with $A_T^{1/3}$, but a more pronounced increase of ≈ 0.5 fm occurs between ^{92}Zr and ^{94}Mo. This is an effect of the quantum number $G_{\text{g.s.}}$ applied for each nucleus, since the use of a lower (or higher) number for $G_{\text{g.s.}}$ results in a lower (or higher) value for the radial parameter of the α + core potential, considering the other parameters as fixed.

For a more comprehensive analysis, the R values for ^{20}Ne, ^{44}Ti, and ^{212}Po have been determined (see Table II) with the same procedures described in Sec. III, except for the choice of $G_{\text{g.s.}} = 20$ for ^{212}Po, which is cited in Ref. [11] as a more appropriate number to describe the experimental spectrum of ^{212}Po in comparison with the quantum number predicted by the Wildermuth condition.

We have made linear fits with one and two parameter(s) for R as a function of $A_T^{1/3}$ and R as a function of $A_\alpha^{1/3} + A_{\text{core}}^{1/3}$. Two sets of nuclei have been considered in the fits: the set of five intermediate mass nuclei and the set of nuclei with α clustering above double shell closure (^{20}Ne, ^{44}Ti, ^{94}Mo, and
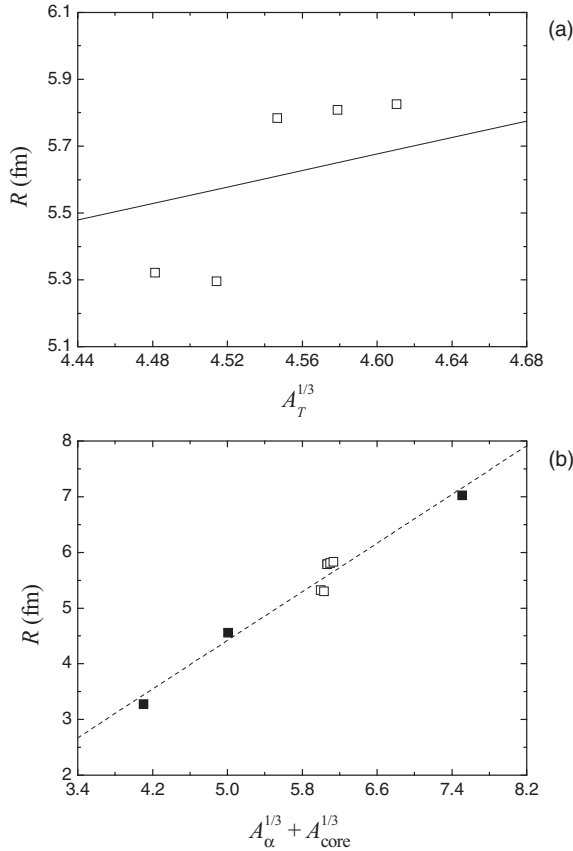
FIG. 3. Values of the parameter R for the nuclei ^{90}Sr, ^{92}Zr, ^{94}Mo, ^{96}Ru, and ^{98}Pd (open squares) as a function of $A_T^{1/3}$ (a) and $A_\alpha^{1/3} + A_{\rm core}^{1/3}$ (b). For a more comprehensive analysis, the R values for ^{20}Ne, ^{44}Ti, and ^{212}Po (full squares) are also shown in (b). The full line shows Eq. (5) fitted to describe the R values of the five intermediate mass nuclei. The dashed line shows Eq. (6) fitted to describe the R values of ^{20}Ne, ^{44}Ti, ^{94}Mo, and ^{212}Po.

^{212}Po). Comparing the fitted functions, it was verified that the relation

$$R = 1.234 \, A_T^{1/3} \, ({\rm fm}) \tag{5}$$

[see Fig. 3(a)] provides a good description of the R values for the five intermediate mass nuclei and also for ^{20}Ne, ^{44}Ti, and ^{212}Po. However, the best fit obtained for the set {^{20}Ne, ^{44}Ti, ^{94}Mo, ^{212}Po} is given by

$$R = 1.092 \big(A_\alpha^{1/3} + A_{\rm core}^{1/3} \big) - 1.041 \, ({\rm fm}), \tag{6}$$

which is shown graphically in Fig. 3(b). The correlation coefficient for the points $(R, A_T^{1/3})$ of the five intermediate mass nuclei is $r \approx 0.882$, and the same measure for the

TABLE II. Values of the radial parameter R and the quantum number $G_{\rm g.s.}$ for ^{20}Ne, ^{44}Ti, and ^{212}Po.

Nucleus	System	R (fm)	$G_{\rm g.s.}$
^{20}Ne	$\alpha + {}^{16}$O	3.272	8
^{44}Ti	$\alpha + {}^{40}$Ca	4.551	12
^{212}Po	$\alpha + {}^{208}$Pb	7.019	20

points $(R, (A_\alpha^{1/3} + A_{\rm core}^{1/3}))$ of the set {^{20}Ne, ^{44}Ti, ^{94}Mo, ^{212}Po} is $r \approx 0.993$. These results confirm the linear trend of the parameter R in relation to the total nuclear radius and the sum of the α cluster and core radii.

B. Ground state bands

Using the $\alpha + $ core potential described in Sec. III, we have calculated the ground state bands for ^{90}Sr, ^{92}Zr, ^{94}Mo, ^{96}Ru, and ^{98}Pd. The obtained levels are compared with the corresponding experimental energies in Fig. 4 (see the label Calc. $V_0 = 220$ MeV). The theoretical bands of the five nuclei give a good overall description of the experimental spectra, if we consider that only the parameter R is varied for each nucleus (see Table I) and the fixed parameters V_0, a, and b have been adjusted [11] to reproduce spectroscopic properties of nuclei of different mass regions. There are experimental levels of ^{92}Zr, ^{94}Mo, and ^{98}Pd with uncertain assignments and the definitive identification of such states is desirable. The experimental levels $E_x = 2.9277$ MeV and $E_x = 3.9543$ MeV of ^{90}Sr do not present identified spins and parities, however, we suggest an association with the theoretical states 6^+ and 8^+, respectively, since these levels and the experimental 4^+ state ($E_x = 1.655\,91$ MeV) are connected by intense γ transitions [20].

The $\alpha + $ core potential produces a quasirotational behavior for the first states of the calculated ground state bands, resulting in a rougher description of the spacing between the 0^+ bandhead and the 2^+ state for the five nuclei. It must be mentioned that this feature is observed in nuclei of different mass regions with the same $\alpha + $ core potential form [11] and other $\alpha + $ core potential forms [9,10,13]. The variation of spacing between the calculated intermediate states is small, while the highest spin states show a compression. Such behavior is typical for the nuclear W.S. $+$ W.S.^{3} potential applied at the intermediate and heavy mass regions, where the calculated bands present high spin members. The difficulty to reproduce simultaneously the spacing between the 0^+ and 2^+ states and higher spin states above 2^+ shows the convenience of choosing the experimental 4^+ state for the fit of the radial parameter R.

The W.S. $+$ W.S.^{3} potential with fixed parameters yields better results than other potential forms used for intermediate mass nuclei. E.g., it is known that the simple Woods-Saxon potential generates an inverted spectrum where the G^+ state has the lowest energy and 0^+ state has the highest energy [17]. The folding potential produces a band with rotational feature, but excessively compressed, and the inclusion of an L-dependent strength parameter is required [17,25]. The $\alpha + $ core potential of shape $(1 + $ Gaussian$) \times$ W.S.^{2} used for ^{94}Mo [13] produces a rotational type band (see Fig. 5), which is incompatible with the respective experimental spectrum. It is observed in Fig. 4 that the experimental spectra of other $N = 52$ nuclei are also quite different from the pure rotational spacing. The W.S. $+$ W.S.^{3} potential with fixed parameters is shown to be favorable mainly to describe the intermediate levels above the 2^+ state, since the rotational behavior of its calculated band attenuates significantly above this level.

Analyzing the calculated positive parity states above the $\alpha + $ core threshold, it is verified that the extension of the effective potential barrier [see Eq. (3)] varies within the
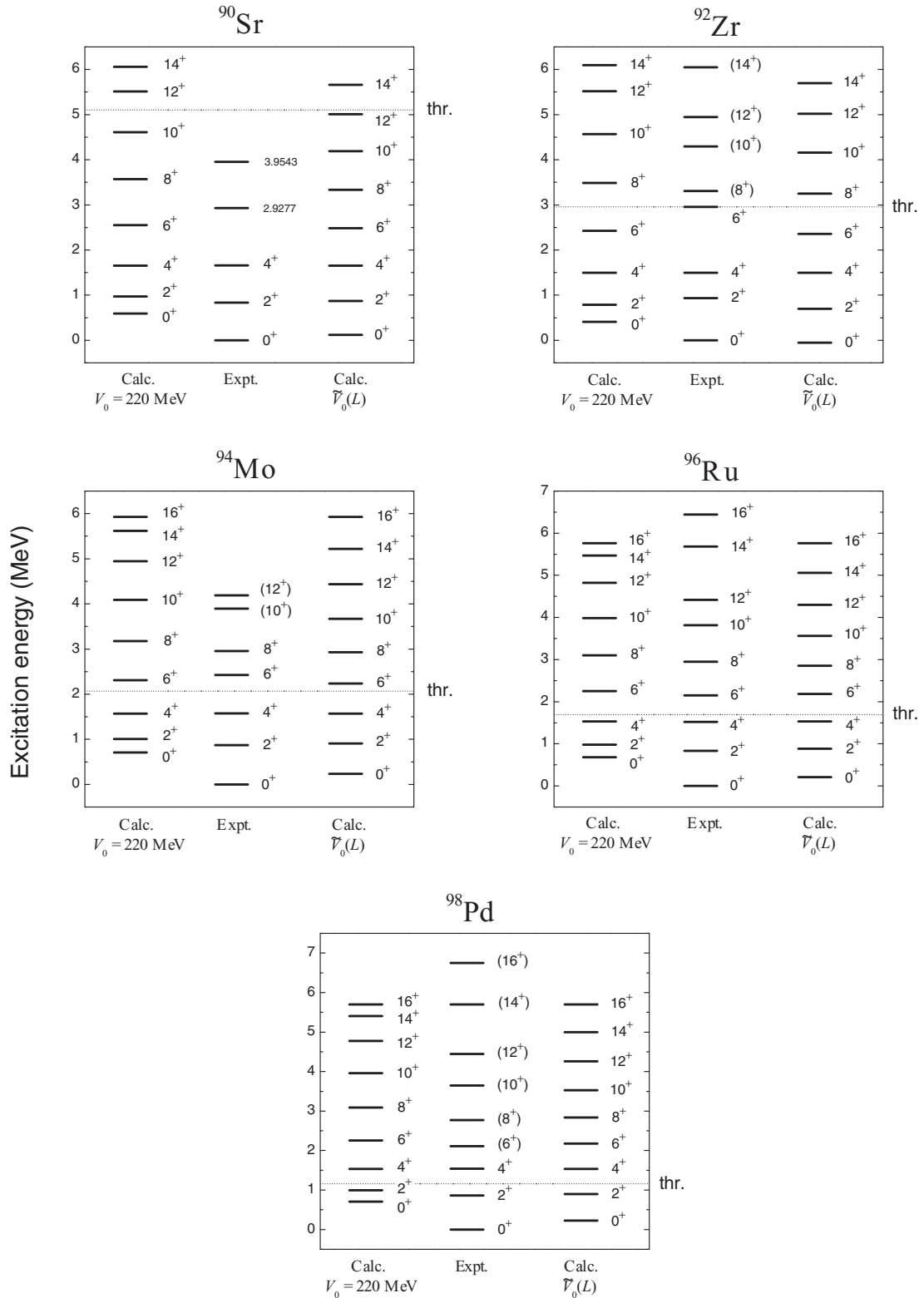
FIG. 4. Calculated α + core energies for the ground state bands of ^{90}Sr ($G = 14$), ^{92}Zr ($G = 14$), ^{94}Mo ($G = 16$), ^{96}Ru ($G = 16$), and ^{98}Pd ($G = 16$) in comparison with the available experimental excitation energies. The label Calc. $V_0 = 220$ MeV indicates the calculated g.s. bands with the fixed depth parameter, and the label Calc. $\tilde{V}_0(L)$ indicates the calculated g.s. bands with the L-dependent depth parameter [see the text for details of $\tilde{V}_0(L)$]. The dotted lines indicate the α + core thresholds. The experimental data are from Refs. [20–24].
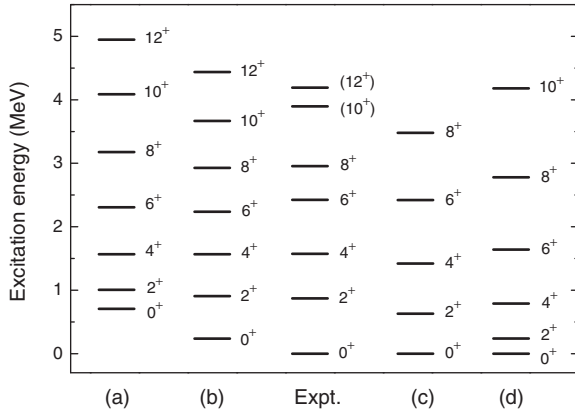
FIG. 5. Comparison of different calculations for the ground state band ($G = 16$) of ^{94}Mo with the experimental excitation energies. Calc. (a) is obtained in this work with the W.S. + W.S.^{3} potential and fixed depth $V_0 = 220$ MeV. Calc. (b) is obtained in this work with the W.S. + W.S.^{3} potential and L-dependent depth parameter (details in the text). Calc. (c) [12,25] is obtained with a double folding potential using a DDM3Y nucleon-nucleon interaction and a L-dependent normalization factor. Calc. (d) [13] is obtained with a phenomenological potential of shape $(1 + \text{Gaussian}) \times \text{W.S.}^2$. The potentials of (c) and (d) were also used to reproduce $\alpha + {}^{90}$Zr elastic scattering data.

FIG. 6. Depths V_0 fitted to reproduce the experimental energy levels of the g.s. bands of ^{90}Sr, ^{92}Zr, ^{94}Mo, ^{96}Ru, and ^{98}Pd as a function of the angular momentum L. The solid line shows the function $\tilde{V}_0(L)$ [see Eq. (7)] chosen for a general description of the graphs $V_0 \times L$. The dotted line indicates the constant value $V_0 = 220$ MeV used for a first description of the spectra. Note that the scale for V_0 shows only very minor variations of approx. $\pm 1.5\%$ from $V_0 = 220$ MeV. The dots accompanied by the symbol (?) are related to the experimental ^{90}Sr levels with unidentified spins and parities, and an association with the corresponding L numbers is suggested (details in the text and Fig. 4).

range 204 fm $< \Delta r <$ 476 fm for the resonant states nearest the threshold, and within the range 31 fm $< \Delta r <$ 114 fm for the highest spin states (14^+ for ^{90}Sr and ^{92}Zr and 16^+ for ^{94}Mo, ^{96}Ru, and ^{98}Pd). The height of the effective potential barrier in relation to the resonant energies varies within the range 13 MeV $< \Delta E <$ 25 MeV for the resonant states nearest the threshold, and within the range 27 MeV $< \Delta E <$ 31 MeV for the highest spin states. These features demonstrate that the positive parity states above the threshold are strongly bound and their resonant behavior is negligible.

Several members of the ground state bands of ^{92}Zr and ^{94}Mo are identified in α-transfer experiments. The ^{92}Zr states from 0^+ to (12^+) are populated in the ^{88}Sr(^{7}Li,$2np\gamma$)^{92}Zr reaction [21,26] and the ^{94}Mo states from 0^+ to 6^+ are populated in the ^{90}Zr(^{16}O,^{12}C γ)^{94}Mo reaction [22,27]. Such experimental information reinforces the choice of the mentioned states for comparison with the calculated bands. The work of Yamaya *et al.* [28] shows the spectrum of ^{94}Mo measured by the ^{90}Zr(^{6}Li,d)^{94}Mo reaction, suggesting that the 0^+, 2^+, 4^+, and 6^+ members of the ground state band of ^{94}Mo are populated in this reaction; however, the same work regards this experiment as unsuccessful because of the strong effect of the ^{12}C and ^{16}O contaminants on the target, which makes the identification of the energy levels very difficult. The main tables of spectroscopic data of ^{90}Sr [20], ^{96}Ru [23], and ^{98}Pd [24] do not present information from α-transfer reactions and new experiments will be useful to verify the experimental levels selected for these three nuclei.

The radial wave functions of the positive parity states have been determined to investigate other properties. A bound state approximation has been used to determine the radial wave functions of the resonant states. For the calculation of the functions, the depth V_0 is adjusted for each state in order
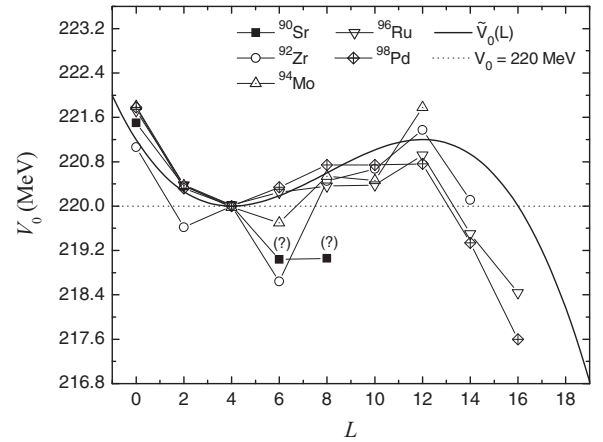
to reproduce the experimental excitation energies of the five nuclei. Observing the values of V_0 in Table III, we note a very small relative variation in comparison with the fixed value (220 MeV) used for the first calculation of the ground state bands. This fact confirms that the fixed depth $V_0 = 220$ MeV is appropriate for an overall description of the spectra and shows that V_0 is weakly dependent on L.

The fitted values of V_0 are shown graphically in Fig. 6 as a function of L. It is noted that, with few exceptions, the variation of V_0 is similar for the five nuclei. There are local minima of V_0 at $L = 4$ and $L = 6$, and local maxima at $L = 12$. Such features are favorable to describe approximately the behavior of V_0 by a function $\tilde{V}_0(L)$. For this purpose, we have chosen a third degree polynomial function which is determined by two previously selected points $(L, \tilde{V}_0)$:

$$\left(L_{\min}, \tilde{V}_0^{\min}\right) = (4,220) \quad \text{and} \quad \left(L_{\max}, \tilde{V}_0^{\max}\right) = (12,221.2).$$

$\tilde{V}_0^{\min}$ and $\tilde{V}_0^{\max}$ are given in MeV. The points $(L_{\min}, \tilde{V}_0^{\min})$ and $(L_{\max}, \tilde{V}_0^{\max})$ are the local minimum and maximum of the function $\tilde{V}_0(L)$, respectively. The values of $L_{\min}$ and $\tilde{V}_0^{\min}$ are appropriate to reproduce the local minima of V_0 for ^{96}Ru and ^{98}Pd and also the decreasing behavior of the graphs $V_0 \times L$ between $L = 0$ and $L = 4$. The values of $L_{\max}$ and $\tilde{V}_0^{\max}$ are appropriate to reproduce approximately the local maxima of V_0 for ^{92}Zr, ^{94}Mo, ^{96}Ru, and ^{98}Pd. Thus one obtains

$$\tilde{V}_0(L) = c_1(L - L_{\min})^3 + c_2(L - L_{\min})^2 + \tilde{V}_0^{\min}, \quad (7)$$

where

$$c_1 = -4.6875 \times 10^{-3} \, \text{MeV} \quad \text{and} \quad c_2 = 0.056\,25 \, \text{MeV}.$$

Equation (7) is shown graphically in Fig. 6. Between $L = 0$ and $L = 12$, the function $\tilde{V}_0(L)$ provides a good general

TABLE III. Calculated values for the rms intercluster separation ($\langle R^2 \rangle^{1/2}$), the ratio of $\langle R^2 \rangle^{1/2}$ to the sum of the experimental rms charge radii of the α cluster and the core [$\langle R^2 \rangle^{1/2}/(\langle r^2 \rangle_\alpha^{1/2} + \langle r^2 \rangle_{\text{core}}^{1/2})$], the reduced α width (γ_α^2) and the dimensionless reduced α width (θ_α^2) for the members of the ground state bands of ^{90}Sr, ^{92}Zr, ^{94}Mo, ^{96}Ru, and ^{98}Pd. The depths V_0 used to fit each state at the corresponding experimental energy (E_x) are also indicated. See the text for explanation about the channel radii. The experimental excitation energies are from Refs. [20–24].

				^{90}Sr (α-^{86}Kr system)		
J^π	E_x (MeV)	V_0 (MeV)	$\langle R^2 \rangle^{1/2}$ (fm)	$\langle R^2 \rangle^{1/2}/(\langle r^2 \rangle_\alpha^{1/2} + \langle r^2 \rangle_{\text{core}}^{1/2})$	γ_α^2 (eV)	θ_α^2 (10^{-6})
0^+	0.000	221.50	4.650	0.794	90.60	408.7
2^+	0.832	220.36	4.652	0.794	95.05	428.8
4^+	1.656	220.01	4.623	0.789	73.58	331.9

				^{92}Zr (α-^{88}Sr system)		
J^π	E_x (MeV)	V_0 (MeV)	$\langle R^2 \rangle^{1/2}$ (fm)	$\langle R^2 \rangle^{1/2}/(\langle r^2 \rangle_\alpha^{1/2} + \langle r^2 \rangle_{\text{core}}^{1/2})$	γ_α^2 (eV)	θ_α^2 (10^{-6})
0^+	0.000	221.06	4.686	0.795	115.51	526.5
2^+	0.935	219.62	4.695	0.796	126.89	578.3
4^+	1.495	220.00	4.652	0.789	89.49	407.9
6^+	2.957	218.64	4.610	0.782	61.56	280.6
8^+	3.309	220.45	4.511	0.765	20.31	92.6
10^+	4.297	220.67	4.426	0.751	5.57	25.4
12^+	4.947	221.37	4.347	0.737	0.84	3.8
14^+	6.046	220.11	4.310	0.731	0.07	0.3

				^{94}Mo (α-^{90}Zr system)		
J^π	E_x (MeV)	V_0 (MeV)	$\langle R^2 \rangle^{1/2}$ (fm)	$\langle R^2 \rangle^{1/2}/(\langle r^2 \rangle_\alpha^{1/2} + \langle r^2 \rangle_{\text{core}}^{1/2})$	γ_α^2 (eV)	θ_α^2 (10^{-6})
0^+	0.000	221.80	5.109	0.859	708.39	3261.8
2^+	0.871	220.37	5.118	0.861	763.03	3513.4
4^+	1.574	219.98	5.087	0.856	615.02	2831.8
6^+	2.423	219.70	5.033	0.847	399.44	1839.2
8^+	2.956	220.54	4.943	0.831	178.00	819.6
10^+	3.897	220.46	4.859	0.817	66.15	304.6
12^+	4.192	221.78	4.765	0.801	14.48	66.7

				^{96}Ru (α-^{92}Mo system)		
J^π	E_x (MeV)	V_0 (MeV)	$\langle R^2 \rangle^{1/2}$ (fm)	$\langle R^2 \rangle^{1/2}/(\langle r^2 \rangle_\alpha^{1/2} + \langle r^2 \rangle_{\text{core}}^{1/2})$	γ_α^2 (eV)	θ_α^2 (10^{-6})
0^+	0.000	221.72	5.103	0.852	595.69	2770.8
2^+	0.833	220.38	5.112	0.853	636.52	2960.7
4^+	1.518	220.02	5.081	0.848	509.85	2371.5
6^+	2.150	220.25	5.020	0.838	310.25	1443.1
8^+	2.950	220.36	4.943	0.825	149.95	697.5
10^+	3.817	220.38	4.861	0.811	54.87	255.2
12^+	4.418	220.92	4.776	0.797	13.11	61.0
14^+	5.681	219.50	4.725	0.789	2.43	11.3
16^+	6.442	218.44	4.702	0.785	0.20	0.9

				^{98}Pd (α-^{94}Ru system)		
J^π	E_x (MeV)	V_0 (MeV)	$\langle R^2 \rangle^{1/2}$ (fm)	$\langle R^2 \rangle^{1/2}/(\langle r^2 \rangle_\alpha^{1/2} + \langle r^2 \rangle_{\text{core}}^{1/2})$	γ_α^2 (eV)	θ_α^2 (10^{-6})
0^+	0.000	221.78	5.101	0.842	497.31	2341.9
2^+	0.863	220.32	5.114	0.844	541.49	2549.9
4^+	1.541	220.00	5.082	0.839	430.80	2028.6
6^+	2.112	220.34	5.019	0.829	256.86	1209.6
8^+	2.773	220.74	4.941	0.816	119.26	561.6
10^+	3.645	220.74	4.859	0.802	43.28	203.8
12^+	4.447	220.76	4.782	0.790	10.90	51.3
14^+	5.699	219.34	4.732	0.781	2.01	9.5
16^+	6.749	217.60	4.715	0.778	0.17	0.8

description of the graphs $V_0 \times L$ and a better approximation for most of the V_0 values in comparison with the constant value $V_0 = 220$ MeV. For $L > 12$, the function gives a rough description of the decreasing behavior of the graphs $V_0 \times L$.

The function $\tilde{V}_0(L)$ has been used for a second calculation of the ground state bands. The nuclear potential form of Eq. (2) is used with $\tilde{V}_0(L)$ as the L-dependent depth factor. The results are compared with the experimental energies in Fig. 4 [see label Calc. $\tilde{V}_0(L)$]. With the L-dependent depth, the variation of spacing between the calculated levels is very small. Such a feature contributes to a better description of the 0^+ bandheads of the five nuclei and the 2^+ states of ^{90}Sr, ^{94}Mo, ^{96}Ru, and ^{98}Pd in comparison with the first calculation where V_0 is fixed. Between $L = 6$ and $L = 12$, most of the states are better described, however, the improvement in comparison with the fixed V_0 calculation is small. For $L = 14$ and $L = 16$, the L-dependent depth does not contribute to a better description of the experimental levels, but avoids the band compression effect for the higher spin states that is incompatible with the experimental spectra of ^{92}Zr, ^{96}Ru and ^{98}Pd.

Figure 5 shows a comparison of different calculations for the ground state band of ^{94}Mo and the experimental spectrum. As mentioned before, the $\alpha + $ core potential of shape $(1 + $ Gaussian$) \times$ W.S.^{2} produces a rotational type spectrum which provides only a rough description of the experimental energies. The double folding potential used in Refs. [12,25] yields a good description of the experimental spectrum between 0^+ and 6^+ by introducing an L-dependent normalization factor. It should be taken into account that the two potential forms mentioned above have been used successfully to reproduce the $\alpha + {}^{90}$Zr elastic scattering data. The W.S. $+$ W.S.^{3} potential with fixed depth $V_0 = 220$ MeV describes roughly the 0^+ bandhead, but the introduction of a weak L dependence by Eq. (7) provides a very good description of the experimental band between the 0^+ and 12^+ states.

The root-mean-square (rms) intercluster separation is given by

$$\langle R^2 \rangle_{G,J}^{1/2} = \left[\int_0^\infty r^2 u_{G,J}^2(r)\, dr \right]^{1/2}, \qquad (8)$$

where $u_{G,J}(r)$ is the normalized radial wave function of a $|G,J\rangle$ state. The value of $\langle R^2 \rangle^{1/2}$ is seen to decrease when one goes from the 0^+ state to the highest spin state of each band (see Table III), except to ^{90}Sr, where there are insufficient known states for a complete analysis. This antistretching effect is found in nuclei of other mass regions where the α-cluster structure is studied, considering different local potential forms [9,10,12]. The same effect is verified by Ohkubo [12] for ^{94}Mo through a double folding potential.

The calculated rms intercluster separations have been used to estimate the rms charge radius of the total nucleus by the equation

$$\langle r^2 \rangle_T = \frac{Z_\alpha}{Z_\alpha + Z_{\text{core}}} \langle r^2 \rangle_\alpha + \frac{Z_{\text{core}}}{Z_\alpha + Z_{\text{core}}} \langle r^2 \rangle_{\text{core}}$$
$$+ \frac{Z_\alpha A_{\text{core}}^2 + Z_{\text{core}} A_\alpha^2}{(Z_\alpha + Z_{\text{core}})(A_\alpha + A_{\text{core}})^2} \langle R^2 \rangle, \qquad (9)$$

where $\langle r^2 \rangle_T^{1/2}$, $\langle r^2 \rangle_\alpha^{1/2}$, and $\langle r^2 \rangle_{\text{core}}^{1/2}$ are the rms charge radii of the total system, the α cluster, and the core, respectively.

TABLE IV. Rms charge radii $\langle r^2 \rangle_T^{1/2}$ calculated for the nuclei ^{90}Sr, ^{92}Zr, ^{94}Mo, and ^{96}Ru through Eq. (9). For each nucleus is shown the ratio of $\langle r^2 \rangle_T^{1/2}$ to the corresponding experimental rms charge radius $(\langle r^2 \rangle_{T \text{ exp}}^{1/2})$ [29].

Total nucleus	$\langle r^2 \rangle_T^{1/2}$ (fm)	$\langle r^2 \rangle_T^{1/2} / \langle r^2 \rangle_{T \text{ exp}}^{1/2}$
^{90}Sr	4.220	0.990
^{92}Zr	4.254	0.988
^{94}Mo	4.322	0.993
^{96}Ru	4.363	0.993

Taking the experimental values [29] of $\langle r^2 \rangle_\alpha^{1/2}$ and $\langle r^2 \rangle_{\text{core}}^{1/2}$ and considering $\langle R^2 \rangle^{1/2}$ as the calculated rms intercluster separation for the ground state 0^+, we find the total rms radii in Table IV. Eq. (9) has not been applied for ^{98}Pd, since there are no experimental values for the rms charge radii of ^{94}Ru and ^{98}Pd. Table IV also shows the ratio of $\langle r^2 \rangle_T^{1/2}$ to the corresponding experimental rms charge radius for each nucleus. The obtained ratios (very close to 1) indicate a high level of agreement between the experimental data and the rms charge radii predicted by the model.

Observing in Table III the ratios

$$\frac{\langle R^2 \rangle^{1/2}}{\langle r^2 \rangle_\alpha^{1/2} + \langle r^2 \rangle_{\text{core}}^{1/2}} \qquad (10)$$

for each nucleus, where $\langle r^2 \rangle_\alpha^{1/2}$ and $\langle r^2 \rangle_{\text{core}}^{1/2}$ are experimental values, we verify a significant overlap between the α cluster and the core for the ground states of the five nuclei. Because of the antistretching effect, the overlap degree of the $\alpha + $ core system increases for higher spin states, so that the α-cluster character of the system is stronger for the first states of the g.s. bands.

A comparison of the same ratios indicates that the set of nuclei with $G_{\text{g.s.}} = 16$ (^{94}Mo, ^{96}Ru, and ^{98}Pd) has a more pronounced α clustering than the set with $G_{\text{g.s.}} = 14$ (^{90}Sr and ^{92}Zr). Concerning the 0^+ ground states of the five nuclei, the ratios $\langle R^2 \rangle^{1/2}/(\langle r^2 \rangle_\alpha^{1/2} + \langle r^2 \rangle_{\text{core}}^{1/2})$ for the $G_{\text{g.s.}} = 16$ nuclei are approximately 6–8% higher than the ratios for the $G_{\text{g.s.}} = 14$ nuclei. In this case, there is a clear effect of the quantum number $G_{\text{g.s.}}$, since the lower value of $G_{\text{g.s.}}$ results in a reduced value for the radial parameter R and, consequently, less extensive radial wave functions.

The radial wave functions are also used for the calculation of the reduced α width [30,31]

$$\gamma_\alpha^2 = \left(\frac{\hbar^2}{2\mu a_c} \right) u^2(a_c) \left[\int_0^{a_c} |u(r)|^2 dr \right]^{-1}, \qquad (11)$$

where μ is the reduced mass of the system, $u(r)$ is the radial wave function of the state, and a_c is the channel radius. In general, a_c lies near the radius of the Coulomb barrier top. It is known that the γ_α^2 value is very sensitive to the choice of the channel radius. As an example, Fig. 7 shows γ_α^2 as a function of a_c for the 0^+, 6^+, and 12^+ states of ^{94}Mo; it is verified that the decrease of γ_α^2 with increasing a_c is of exponential type (and linear type with the $\log_{10}$ scale for γ_α^2) from ≈ 7 fm.
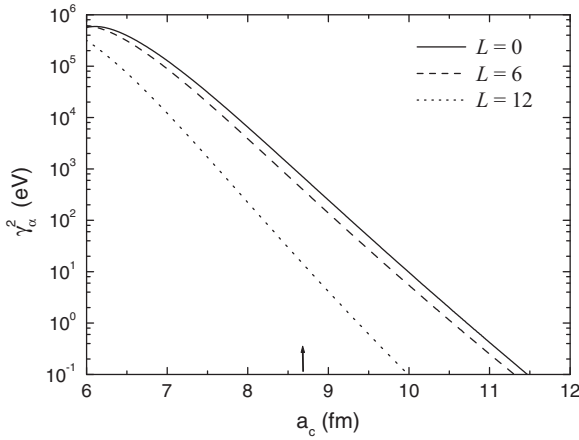
FIG. 7. Reduced α width (γ_α^2) as a function of the channel radius (a_c) for the 0^+, 6^+, and 12^+ states of ^{94}Mo. The arrow indicates the value of a_c obtained by Eq. (12). The γ_α^2 axis is represented in a $\log_{10}$ scale.

In this work, a procedure that avoids an arbitrary choice of channel radius is used. The value of a_c is given by the relation

$$a_c = 1.295\left(A_\alpha^{1/3} + A_{\text{core}}^{1/3}\right) + 0.824, \quad (12)$$

obtained from a linear fit (see Fig. 8) that considers other channel radii used for different α + core systems in the literature [10,12,32]. The dimensionless reduced α width θ_α^2 is defined as the ratio of γ_α^2 to the Wigner limit, that is,

$$\theta_\alpha^2 = \frac{2\mu a_c^2}{3\hbar^2}\gamma_\alpha^2. \quad (13)$$

Qualitatively, a large value of $\theta_\alpha^2 (\approx 1)$ is interpreted as an evidence of a high degree of α clustering.

The g.s. bands of ^{92}Zr, ^{94}Mo, ^{96}Ru, and ^{98}Pd show a rapid decrease of γ_α^2 with the increasing spin. In agreement with the analysis of the rms intercluster separations, the behavior of γ_α^2 suggests a stronger α-cluster character for the first members
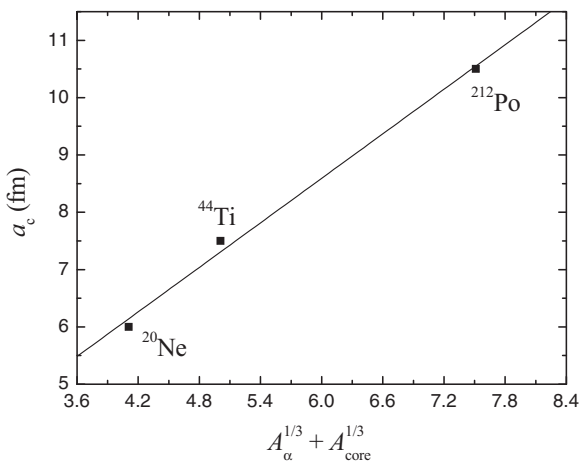

FIG. 8. Channel radii employed in different works for the α + core systems in ^{20}Ne [30,32], ^{44}Ti [10], and ^{212}Po [12] as a function of $A_\alpha^{1/3} + A_{\text{core}}^{1/3}$. The full line shows the linear function fitted for the three radii. See the text for details of the linear function.

of these bands. For the five nuclei, the dimensionless reduced α widths θ_α^2 present a very small fraction of the Wigner limit, even for the first members of the band, indicating a general weak α-cluster character for the g.s. bands.

The effect of the quantum number G on θ_α^2 is analogous to that observed for the ratio of Eq. (10). The set of nuclei with $G_{\text{g.s.}} = 16$ present θ_α^2 values that are approximately one order of magnitude higher than the corresponding θ_α^2 values for the set with $G_{\text{g.s.}} = 14$. Therefore, in addition to the results obtained for the rms radii, it is indicated that the set with $G_{\text{g.s.}} = 16$ has a higher α-cluster degree in comparison with the $G_{\text{g.s.}} = 14$ set.

Comparing the J^π states of the five nuclei in Table III, it is noted that ^{94}Mo has the highest θ_α^2 values. This result corroborates the consideration of ^{94}Mo as the preferential nucleus for α clustering in its mass region.

The model also allows the calculation of the $B(E2)$ transition rates between the states of an α-cluster band. In the case where the cluster and the core have zero spins, this quantity is given by

$$B(E2; G, J \rightarrow J-2) = \frac{15}{8\pi}\beta_2^2 \frac{J(J-1)}{(2J+1)(2J-1)}\langle r_{J,J-2}^2\rangle^2, \quad (14)$$

where

$$\langle r_{J,J-2}^2\rangle = \int_0^\infty r^2 u_{G,J}(r) u_{G,J-2}(r)dr, \quad (15)$$

β_2 is the recoil factor, given by

$$\beta_2 = \frac{Z_\alpha A_{\text{core}}^2 + Z_{\text{core}} A_\alpha^2}{(A_\alpha + A_{\text{core}})^2}; \quad (16)$$

$u_{G,J}(r)$ and $u_{G,J-2}(r)$ are the radial wave functions of the initial $|G,J\rangle$ state and final $|G,J-2\rangle$ state, respectively.

The calculated $B(E2)$ transition rates for the ground state bands are presented in Table V. A comparison of the calculated values for the five nuclei and the experimental data shows that the model can reproduce, with few exceptions, the correct order of magnitude of the experimental $B(E2)$ values without the use of effective charges. These results may be considered satisfactory since, in shell-model calculations for medium-heavy nuclei [33,34], large effective charges are necessary to reproduce the order of magnitude of the experimental data.

Observing the $2^+ \rightarrow 0^+$ and $4^+ \rightarrow 2^+$ transitions for the nuclei ^{90}Sr, ^{92}Zr, ^{94}Mo, and ^{96}Ru, it is noted that the experimental $B(E2)$ rates for ^{94}Mo and ^{96}Ru are ≈ 2–$6\times$ higher than the experimental rates for ^{90}Sr and ^{92}Zr. This fact indicates that the application of the quantum numbers $G_{\text{g.s.}} = 14$ for ^{90}Sr and ^{92}Zr, and $G_{\text{g.s.}} = 16$ for ^{94}Mo and ^{96}Ru, is favorable for a better description of the experimental transition rates. The functions $u_{G,J}(r)$ with $G_{\text{g.s.}} = 16$ are more extensive at the surface region than the functions $u_{G,J}(r)$ with $G_{\text{g.s.}} = 14$, which results in higher values for the calculated $B(E2)$ rates of ^{94}Mo and ^{96}Ru.

The $B(E2)$ values calculated by Mohr [17] with a double folding nuclear potential, also without effective charges, are ≈ 1.3–$1.4\times$ higher than the values of this work for ^{90}Sr and ^{92}Zr, and $\approx 1.15\times$ higher for ^{94}Mo and ^{96}Ru. Compared to

TABLE V. Comparison of the calculated $B(E2)$ transition rates for the ground state bands of ^{90}Sr, ^{92}Zr, ^{94}Mo, ^{96}Ru, and ^{98}Pd with the corresponding experimental data [20–24]. The calculated values have been obtained without effective charges.

^{90}Sr (α-^{86}Kr system)		
J^{π}	$B(E2; J \rightarrow J - 2)$ (W.u.)	$B(E2)_{\text{exp.}}$ (W.u.)
2^+	5.569	8.5(24)
4^+	7.635	5.2(9)
^{92}Zr (α-^{88}Sr system)		
J^{π}	$B(E2; J \rightarrow J - 2)$ (W.u.)	$B(E2)_{\text{exp.}}$ (W.u.)
2^+	5.623	6.4(6)
4^+	7.661	4.05(12)
6^+	7.727	$\geqslant$0.00098
8^+	6.610	3.59(22)
10^+	5.268	
12^+	3.569	$\geqslant$0.056
14^+	1.859	
^{94}Mo (α-^{90}Zr system)		
J^{π}	$B(E2; J \rightarrow J - 2)$ (W.u.)	$B(E2)_{\text{exp.}}$ (W.u.)
2^+	7.757	16.0(4)
4^+	10.738	26(4)
6^+	10.898	
8^+	9.798	0.0049(8)
10^+	8.303	
12^+	6.237	
^{96}Ru (α-^{92}Mo system)		
J^{π}	$B(E2; J \rightarrow J - 2)$ (W.u.)	$B(E2)_{\text{exp.}}$ (W.u.)
2^+	7.539	18.4(4)
4^+	10.430	20.7(15)
6^+	10.512	14(5)
8^+	9.584	6.0(22)
10^+	8.098	12.7(15)
12^+	6.190	13.1(19)
14^+	4.341	2.63(23)
16^+	2.186	>11
^{98}Pd (α-^{94}Ru system)		
J^{π}	$B(E2; J \rightarrow J - 2)$ (W.u.)	$B(E2)_{\text{exp.}}$ (W.u.)
2^+	7.364	
4^+	10.195	
6^+	10.253	
8^+	9.315	(without exp.
10^+	7.882	data)
12^+	6.097	
14^+	4.257	
16^+	2.179	

Ref. [17], the present work produces results closer to the experimental values only for ^{90}Sr ($4^+ \rightarrow 2^+$ transition) and ^{92}Zr. In general, it can be stated roughly that the two works produce similar results in comparison with the experimental $B(E2)$ rates.

C. Negative parity bands

The comparison of theoretical negative parity bands with the experimental spectra is more difficult because of the scarce experimental negative parity levels with definite assignments. Previous works [12,14,17] discuss the existence of an $\alpha +$ core negative parity band for ^{94}Mo and indicate that the 1^- bandhead should lie at $E_x = 6$–7 MeV, however, such predictions are not compared with experimental energies of ^{94}Mo. Therefore, at this stage, any calculation concerning the negative parity bands of the studied nuclei should be interpreted as a theoretical prediction that lacks complementary experimental information.

In this work, we have selected the lowest negative parity levels connected by $E2$ transitions (or possible $E2$ transitions) for a comparison with the calculated negative parity bands, which are shown in Fig. 9. The quantum number $G = 15$ is applied to ^{92}Zr and $G = 17$ is applied to ^{94}Mo, ^{96}Ru, and ^{98}Pd. The experimental spectrum of ^{90}Sr [20] presents insufficient data concerning negative parity levels and a comparison with the theoretical negative parity band is unfeasible. The values for the parameters a, b, and R are the same used for the calculation of the g.s. bands, while a depth $V_0 = 238$ MeV is applied to the negative parity bands of the four nuclei. The calculated bands provide a good description of the spacings between most of the experimental energy levels. In the case of the experimental $15^{(-)}$ and $17^{(-)}$ states of ^{96}Ru, the energy spacing is roughly described because of the compression of the theoretical band at the higher spin states. The individual analysis of the four negative parity bands shows that $V_0 = 237$ MeV and $V_0 = 239$ MeV are more appropriate depths to describe the experimental spectra of ^{98}Pd and ^{92}Zr, respectively.

Analyzing the calculated negative parity states above the $\alpha +$ core threshold, it is verified that the extension of the effective potential barrier varies within the range 107 fm $< \Delta r < 635$ fm for the resonant states nearest the threshold, and within the range 25 fm $< \Delta r < 29$ fm for the highest spin states (15^- for ^{92}Zr and 17^- for ^{94}Mo, ^{96}Ru, and ^{98}Pd). The height of the effective potential barrier in relation to the resonant energies varies within the range 13 MeV $< \Delta E < 17$ MeV for the resonant states nearest the threshold, and within the range 28 MeV $< \Delta E < 32$ MeV for the highest spin states. Therefore, the negative parity bands repeat the feature of the ground state bands in which the states above the threshold are practically bound.

Regarding the experimental energy levels, the three negative parity states of ^{92}Zr are populated in the ^{88}Sr(^{7}Li,$2np\gamma$)^{92}Zr reaction [21,26], therefore, being favorable candidates for an association with the calculated α-cluster states. There is no information from α-transfer reactions for the selected negative parity states of ^{94}Mo, ^{96}Ru, and ^{98}Pd [22–24].

The depth $V_0 = 238$ MeV is $\approx$8.2% higher than the depth $V_0 = 220$ MeV used to describe the g.s. bands, indicating a moderate parity dependence for the $\alpha +$ core potential. The variation of the depth parameter for different bands is also observed in other $\alpha +$ core systems [9,35,36]. E.g., a calculation of the α-cluster structure in light nuclei [9] using a folding nuclear potential with a depth parameter $\bar{f}$ shows
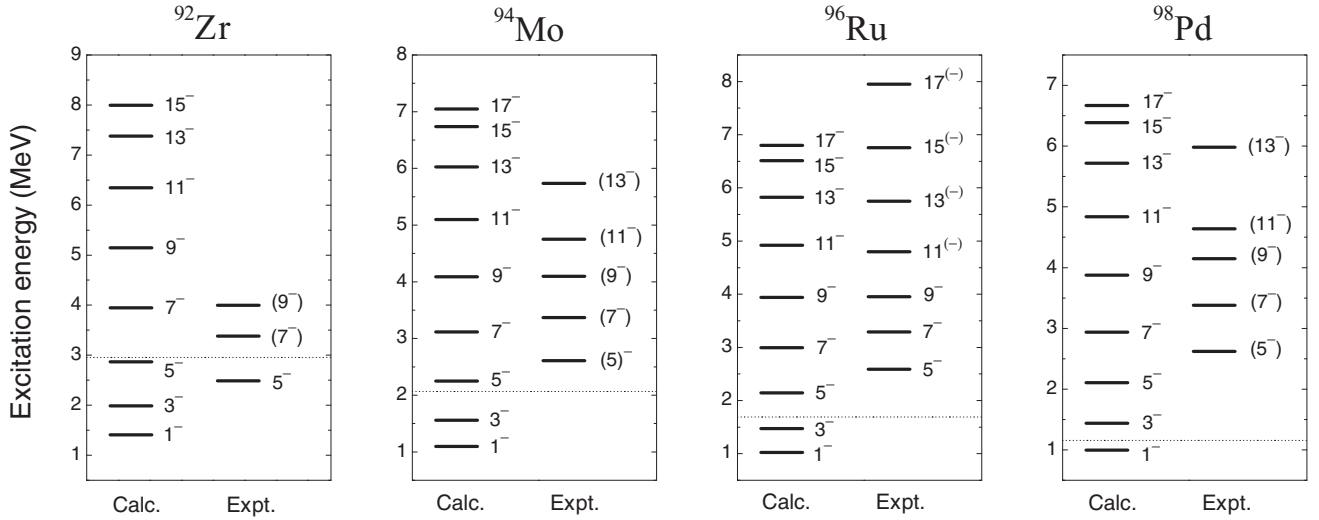
FIG. 9. Calculated α + core energies for the negative parity bands of ^{92}Zr ($G = 15$), ^{94}Mo ($G = 17$), ^{96}Ru ($G = 17$), and ^{98}Pd ($G = 17$) in comparison with the available experimental levels. The dotted lines indicate the α + core thresholds. A depth $V_0 = 238$ MeV was applied. The experimental data are from Refs. [21–24].

that the values of $\overline{f}$ for the negative parity bands of ^{16}O and ^{20}Ne ($G = 9$) are, respectively, $\approx 8.8\%$ and $\approx 7.1\%$ higher than the values of the same parameter for the corresponding positive parity bands ($G = 8$).

Because of the enhanced value of V_0, the bandheads of the theoretical negative parity bands lie close to $E_x = 1$ MeV, which differs from previous predictions for ^{94}Mo [12,14,17]. According to the criterion adopted to select the experimental levels, there are no experimental 1^- and 3^- states for comparison with the calculated bands (see Fig. 9). An experimental 3^- state at $E_x = 2.340$ MeV is present in the spectrum of ^{92}Zr, however, such a state is not connected with the first 5^- state ($E_x = 2.486$ MeV) by a γ transition. The same condition occurs for the experimental 3^- ($E_x = 2.534$ MeV) and $(5)^-$ ($E_x = 2.611$ MeV) states of ^{94}Mo. It is possible that the theoretical 1^- states are experimentally nonexistent near the predicted energies, since the spectra measured by several reactions for the studied nuclei [21–24] do not indicate the presence of a 1^- state around $E_x = 1$ MeV. However, the low energy location of the calculated negative parity bands is mainly justified by the presence of the 5^-, (7^-), and (9^-) experimental levels of ^{92}Zr from $E_x \approx 2.5$ MeV, which are populated in a α-transfer reaction. Additionally, the similar features of the spectra favor a unified description of the negative parity bands of the four nuclei. Further experimental data are essential for a better evaluation of the calculations described in this section.

V. RELATION WITH α + CORE OPTICAL POTENTIALS

The α + core potential may be employed as the real part of an optical potential for the analysis of α elastic scattering. However, is often necessary to readjust one or more parameters of the potential for a satisfactory description of the experimental α-scattering data. The adjustment of the parameters of the imaginary part of the optical potential is also important in this procedure. The works of Buck *et al.* [16,37]

show that the W.S. + W.S.^{3} potential may be used successfully to describe the data of α elastic scattering on nuclei ^{16}O, ^{40}Ca, and ^{208}Pb. Therefore, it is interesting to verify if the α + core potentials discussed in this work can be applied in the same way.

Two important quantities used for describing an optical potential are the volume integral per nucleon pair,

$$ J_R = \frac{4\pi}{A_\alpha A_{\text{core}}} \int_0^\infty V_N(r) r^2 \, dr, \qquad (17) $$

and the root-mean-square (rms) radius associated with the potential,

$$ r_{\text{rms}, R} = \left[\frac{\int_0^\infty V_N(r) r^4 \, dr}{\int_0^\infty V_N(r) r^2 \, dr} \right]^{1/2}. \qquad (18) $$

Equations (17) and (18) refer specifically to the nuclear real part of the optical potential.

Table VI shows the J_R and $r_{\text{rms}, R}$ values calculated for the α + core potentials of this work, with the depths applied to

TABLE VI. Calculated values of the volume integral per nucleon pair (J_R) and root-mean-square radius ($r_{\text{rms}, R}$) for the α + core nuclear potentials employed in this work.

Nucleus	V_0 (MeV)	J_V (MeV fm³)	$r_{\text{rms}, R}$ (fm)
^{90}Sr	220	254.1	4.697
^{90}Sr	238	274.8	4.697
^{92}Zr	220	244.8	4.682
^{92}Zr	238	264.8	4.682
^{94}Mo	220	310.5	4.974
^{94}Mo	238	335.9	4.974
^{96}Ru	220	307.5	4.988
^{96}Ru	238	332.6	4.988
^{98}Pd	220	303.6	4.998
^{98}Pd	238	328.4	4.998

the positive ($V_0 = 220$ MeV) and negative ($V_0 = 238$ MeV) parity bands. As usual, the negative sign of J_R is omitted.

Reference [38] analyzes the α elastic scattering on ^{90}Zr at the energies $E_{\alpha,\text{lab}} = 31.0$, 59.1, 104.0, and 141.7 MeV using a double folding nuclear potential with DDM3Y interaction; for these energies, the values $J_R \approx 270$–335 MeV fm^3 and $r_{\text{rms},R} \approx 5.0$ fm have been obtained. The J_R values obtained in the present work for ^{94}Mo are within the range mentioned previously, and the radius $r_{\text{rms},R}$ obtained in the present work is in excellent agreement with those from Ref. [38]. The works of Ohkubo [12] and Michel, Reidemeister, and Ohkubo [13], which use different forms of $\alpha + {}^{90}$Zr nuclear potential to describe the α elastic scattering data and energy levels, find J_R values very close to the ones obtained in this work for ^{94}Mo.

References [39,40] analyze the α elastic scattering on ^{92}Mo at the energies $E_{\text{c.m.}} \approx 13$, 16, and 19 MeV, also using a double folding nuclear potential with DDM3Y interaction and different parametrizations for the imaginary part of the optical potential. The two references show volume integral values in the range $J_R \approx 320$–360 MeV fm^3 and rms radii in the range $r_{\text{rms},R} \approx 4.9$–$5.1$ fm. The J_R value obtained in this work for ^{96}Ru with $V_0 = 220$ MeV is very close to the range mentioned before, while the J_R value with $V_0 = 238$ MeV is within the same range. The calculated value of $r_{\text{rms},R}$ for ^{96}Ru is also in excellent agreement with those mentioned in Refs. [39,40].

References [38,39] indicate that there is a systematic behavior of J_R for α elastic scattering in different mass regions, resulting in values in the range $J_R \approx 320$–370 MeV fm^3 for almost all analyzed energies around the Coulomb barrier. Therefore, the J_R values calculated in the present work for ^{90}Sr and ^{92}Zr are below the mentioned range. This demonstrates that the choice of the quantum number G can strongly change the J_R value for a certain $\alpha + $ core potential. However, one cannot state in advance that the $\alpha + {}^{86}$Kr and $\alpha + {}^{88}$Sr potentials are unsuitable for description of α elastic scattering at low energies, since the reproduction of the angular distributions also depends on the fit of the parameters of the imaginary part of the optical potential. E.g., the work of Buck *et al.* [16] states that it is possible to describe the data from α elastic scattering on ^{208}Pb at low energies with different fits of optical potential parameters, and such fits are related to different quantum numbers $G_{\text{g.s.}}$.

As ^{94}Ru is an unstable nucleus, the values of J_R and $r_{\text{rms},R}$ for the $\alpha + {}^{94}$Ru system are not compared with other references. The use of the $\alpha + $ core potentials of this work for analysis of α elastic scattering data is a project to be performed in a next stage.

VI. CONCLUSIONS

The α-cluster structure in the nuclei ^{90}Sr, ^{92}Zr, ^{94}Mo, ^{96}Ru, and ^{98}Pd was investigated through a local $\alpha + $ core potential. A good account of the experimental ground state bands of the five nuclei is given with only one variable radial parameter R. Such a parameter has approximately a linear relation with the total nuclear radius and with the sum of the α cluster and core radii. An analysis of the depth parameter V_0 shows a weak dependence on the angular momentum L,

described satisfactorily by a polynomial function $\tilde{V}_0(L)$. The rms intercluster separations and reduced α widths calculated for the ground state bands indicate a decrease of the α-cluster intensity with the increasing spin, and that the nuclei associated with the quantum number $G_{\text{g.s.}} = 16$ (^{94}Mo, ^{96}Ru, and ^{98}Pd) have a significantly higher degree of α clustering than those with $G_{\text{g.s.}} = 14$ (^{90}Sr and ^{92}Zr). The $B(E2)$ transition rates calculated for the ground state bands reproduce the order of magnitude of almost all experimental data without the use of effective charges. It is verified that the employment of $G_{\text{g.s.}} = 14$ for ^{90}Sr and ^{92}Zr and $G_{\text{g.s.}} = 16$ for ^{94}Mo and ^{96}Ru is favorable for a better description of the experimental transition rates.

The calculated negative parity bands provide a good account of the spacings between most of the experimental levels, considering that only the depth parameter was changed from the value employed for the ground state bands; this change indicates a moderate parity dependence for the $\alpha + $ core potential. For the moment, the calculations for the negative parity bands should be interpreted as an exploratory attempt to describe the available experimental data, since many theoretical levels could not be compared to experimental levels or were associated with undefined experimental assignments.

The $\alpha + $ core potentials applied in this work were used to calculate the volume integral per nucleon pair and rms radius. The J_R values calculated for the $\alpha + {}^{90}$Zr and $\alpha + {}^{92}$Mo potentials, referring to the positive and negative parity bands, are compatible or very close to those obtained from the respective optical potentials of α elastic scattering at several energies [38–40]. The calculated rms radii are in excellent agreement with those obtained from the same optical potentials. These results give a strong indication that the $\alpha + {}^{90}$Zr and $\alpha + {}^{92}$Mo potentials of this work may be used to describe α elastic scattering data. Due to the lower $G_{\text{g.s.}}$ number for ^{90}Sr and ^{92}Zr, the values of J_R for the $\alpha + {}^{86}$Kr and $\alpha + {}^{88}$Sr potentials are slightly below the range expected for α-scattering energies around the Coulomb barrier.

The main conclusion of the present work is that the even-even $N = 52$ nuclei around ^{94}Mo present similar $\alpha + $ core structures. In addition, it is pointed out that the α-cluster model can be extended successfully for other nuclei of the intermediate mass region. New experimental data, mainly from α-transfer reactions, will be very important for a better evaluation of the calculated α-cluster states. The local potential model should be used in a next work for investigating the α-cluster structure in other nuclei of the same mass region. Another project to be performed is the application of the $\alpha + $ core potentials of this work for analysis of α elastic scattering data.

[1] M. Ismail and A. Adel, Phys. Rev. C **90**, 064624 (2014).

[2] Yibin Qian and Zhongzhou Ren, Phys. Rev. C **90**, 064308 (2014).

[3] T. T. Ibrahim and S. M. Wyngaardt, J. Phys. G: Nucl. Part. Phys. **41**, 055111 (2014).

[4] S. B. Duarte and N. Teruya, Phys. Rev. C **85**, 017601 (2012).

[5] Bo Zhou, Y. Funaki, H. Horiuchi, Zhongzhou Ren, G. Röpke, P. Schuck, A. Tohsaki, Chang Xu, and T. Yamada, Phys. Rev. Lett. **110**, 262501 (2013).

[6] M. Girod and P. Schuck, Phys. Rev. Lett. **111**, 132503 (2013).

[7] W. B. He, Y. G. Ma, X. G. Cao, X. Z. Cai, and G. Q. Zhang, Phys. Rev. Lett. **113**, 032506 (2014).

[8] T. Baba, Y. Chiba, and M. Kimura, Phys. Rev. C **90**, 064319 (2014).

[9] B. Buck, C. B. Dover, and J. P. Vary, Phys. Rev. C **11**, 1803 (1975).

[10] F. Michel, G. Reidemeister, and S. Ohkubo, Phys. Rev. C **37**, 292 (1988).

[11] B. Buck, A. C. Merchant, and S. M. Perez, Phys. Rev. C **51**, 559 (1995).

[12] S. Ohkubo, Phys. Rev. Lett. **74**, 2176 (1995).

[13] F. Michel, G. Reidemeister, and S. Ohkubo, Phys. Rev. C **61**, 041601 (2000).

[14] M. A. Souza and H. Miyake, Braz. J. Phys. **35**, 826 (2005).

[15] F. Hoyler, P. Mohr, and G. Staudt, Phys. Rev. C **50**, 2631 (1994).

[16] B. Buck, J. C. Johnston, A. C. Merchant, and S. M. Perez, Phys. Rev. C **53**, 2841 (1996).

[17] P. Mohr, Open Nucl. & Part. Phys. J. **1**, 1 (2008).

[18] G. Audi, A. H. Wapstra, and C. Thibault, Nucl. Phys. A **729**, 337 (2003); http://amdc.in2p3.fr/web/masseval.html

[19] K. Wildermuth and Y. C. Tang, *A Unified Theory of the Nucleus* (Academic, New York, 1977).

[20] E. Browne, Nucl. Data Sheets **82**, 379 (1997).

[21] C. M. Baglin, Nucl. Data Sheets **113**, 2187 (2012).

[22] D. Abriola and A. A. Sonzogni, Nucl. Data Sheets **107**, 2423 (2006).

[23] D. Abriola and A. A. Sonzogni, Nucl. Data Sheets **109**, 2501 (2008).

[24] B. Singh and Z. Hu, Nucl. Data Sheets **98**, 335 (2003).

[25] F. Michel, S. Ohkubo, and G. Reidemeister, Prog. Theor. Phys. Suppl. **132**, 7 (1998).

[26] B. A. Brown, D. B. Fossan, P. M. S. Lesser, and A. R. Poletti, Phys. Rev. C **14**, 602 (1976).

[27] H. Bohn, Gisela Daniel, M. R. Maier, P. Kienle, J. G. Cramer, and D. Proetel, Phys. Rev. Lett. **29**, 1337 (1972).

[28] T. Yamaya, K. Katori, M. Fujiwara, S. Kato, and S. Ohkubo, Prog. Theor. Phys. Suppl. **132**, 73 (1998).

[29] I. Angeli, At. Data Nucl. Data Tables **87**, 185 (2004).

[30] A. Arima and S. Yoshida, Nucl. Phys. A **219**, 475 (1974).

[31] G. Michaud, L. Scherk, and E. Vogt, Phys. Rev. C **1**, 864 (1970).

[32] Y. Fujiwara, H. Horiuchi, K. Ikeda, M. Kamimura, K. Kato, Y. Suzuki, and E. Uegaki, Suppl. Prog. Theor. Phys. **68**, 29 (1980).

[33] Chang-hua Zhang, Shun-jin Wang, and Jin-nan Gu, Phys. Rev. C **60**, 054316 (1999).

[34] A. F. Lisetskiy, N. Pietralla, C. Fransen, R. V. Jolos, and P. von Brentano, Nucl. Phys. A **677**, 100 (2000).

[35] B. Buck, A. C. Merchant, and S. M. Perez, Nucl. Phys. A **652**, 211 (1999).

[36] F. Michel, J. Albinski, P. Belery, T. Delbar, G. Gregoire, B. Tasiaux, and G. Reidemeister, Phys. Rev. C **28**, 1904 (1983).

[37] B. Buck, J. C. Johnston, A. C. Merchant, and S. M. Perez, Phys. Rev. C **52**, 1840 (1995).

[38] U. Atzrott, P. Mohr, H. Abele, C. Hillenmayer, and G. Staudt, Phys. Rev. C **53**, 1336 (1996).

[39] P. Mohr, G. G. Kiss, Zs. Fülöp, D. Galaviz, Gy. Gyürky, and E. Somorjai, At. Data Nucl. Data Tables **99**, 651 (2013).

[40] Zs. Fülöp *et al.*, Phys. Rev. C **64**, 065805 (2001).